Iteration over event space in time-to-first-spike spiking neural networks for Twitter bot classification*

Mateusz Pabian^{a,*}, Dominik Rzepka^a, Mirosław Pawlak^{b,a,c}

Abstract

This study proposes a framework that extends existing time-coding time-to-first-spike spiking neural network (SNN) models to allow processing information changing over time. We explain spike propagation through a model with multiple input and output spikes at each neuron, as well as design training rules for end-to-end backpropagation. This strategy enables us to process information changing over time. The model is trained and evaluated on a Twitter bot detection task where the time of events (tweets and retweets) is the primary carrier of information. This task was chosen to evaluate how the proposed SNN deals with spike train data composed of hundreds of events occurring at timescales differing by almost five orders of magnitude. The impact of various parameters on model properties, performance and training-time stability is analyzed.

Keywords: spiking neural networks, event-based computing, supervised bot detection

Email address: pabian@agh.edu.pl (Mateusz Pabian)

^aDepartment of Measurement and Electronics, AGH University of Krakow, al. Mickiewicza 30, 30-059, Kraków, Poland

^bDepartment of Electrical and Computer Engineering, University of Manitoba, 75 Chancellors Circle, R3T 5V6, Winnipeg, Canada

^cInformation Technology Institute, University of Social Sciences, ul. Sienkiewicza 9, 90-113, Łódź, Poland

 $^{^{\}star}\mathrm{This}$ work was supported by the Polish National Center of Science under Grant DEC-2017/27/B/ST7/03082.

^{*}Corresponding author

1. Introduction

Spiking neural networks (SNN) differ from classic artificial neural networks in how the signal is represented and propagated through the network. This in turn determines their applicability to event-driven types of data (i.e., characterized by event occurrence as the primary information carrier, or data that can be represented in this form by a proper encoding). SNN process data using impulses which are asynchronously propagated through the entire network [1, 2]. This processing scheme stands in contrast to the classic artificial neural networks which require that all neurons within a single layer must finish their computation before the signal flows to the subsequent layer. Overall, the aim of SNN is to model biological networks in a much more principled way. The training rules for the SNN generally fall into one of three categories: network conversion (mapping each component of the source network to its spiking equivalent) [3, 4, 5], synaptic-plasticity-aware training (taking advantage of long-term potentiation and long-term depression effects) [6, 7], or training with backpropagation [8, 9, 10]. The latter approach necessitates formulating custom training rules that take into account the fact that the activation function of biological neurons - "all-or-nothing" principle - is not differentiable. Hybrid conversionbackpropagation approaches have also been explored [11].

There are several factors that inhibit research on the SNN. One of them is the availability of event data. In case such dataset is unavailable (due to its proprietary nature or when the original signal exists in the analog domain), researchers can opt to transform existing sets of data to an event structure [12, 13]. Regardless of how the event data is obtained, it is possible to compare the SNN with nonspiking models trained on the same task. Another inhibiting factor is the computational complexity of simulating the SNN on typical hardware. Fortunately, the research on spiking neural networks goes hand-in-hand with the development of dedicated neuromorphic hardware [14].

In this paper we use backpropagation to train an SNN based on the timeto-first-spike neurons introduced in [8]. We address one of the limitations of this model related to the infinitely long neuron refractory period $\tau_{\rm ref}$. This shortcoming means that every neuron in the model can elicit at most one spike during a single input example presentation. Overcoming this limitation allows us to design a model that is able to process information changing over time. Crucially, the proposed signal propagation and network training rules are truly event-centric, evaluating the state of the model at each event rather than at fixed points in time determined by the simulation grid. We evaluate our approach by training a classification network on real-life dataset of legitimate and automated Twitter user activity [15]. We choose this data for several reasons. First of all, each record is described only in terms of the time of event without any auxiliary information (such as tweet content and sentiment). Secondly, spike trains formed for each record are several hundred events long. Lastly, the events occur at timescales differing by many orders of magnitude. This allows us to assess the feasibility of the proposed approach in scenarios commonly encountered when processing this type of data.

This paper is structured as follows. In Sections 1.1 and 1.2 we give a brief overview of backpropagation-based algorithms for training time-coding SNN, as well as introduce the Twitter bot detection problem. Section 2 describes the signal propagation and training rules for the proposed SNN, with the main contributions outlined in Sections 2.2 and 2.3. The dataset properties, training data selection and preprocessing steps are described in Section 3. Finally, we summarize our experimental results in Section 4, showing the impact of model parameters on network properties and performance.

1.1. Related works on backpropagation-based training of SNN

Training artificial spiking neural networks with backpropagation leverages existing methods, algorithms and best practices developed for artificial non-spiking neural networks and deep learning. In doing so it forgoes biological plausibility, evident in training methods based on spike-timing-dependent plasticity effects [6].

One of the first proposed gradient-descent-based learning rules for timing-

encoding networks was the SpikeProp algorithm [16] and its variants. It established key traits of backpropagation algorithms present in subsequent works. In particular, the algorithm has the following characteristics: 1) the SNN is simulated over a finite time window with a fixed time step, recording changes in the internal state (membrane voltage, synaptic current) of all neurons during the forward pass and 2) approximating (smoothing) the spike-generation function to avoid a discontinuous derivative (unless this discontinuity is ignored and treated as noise, as in [17]). Backpropagation-based approaches for training time-coding SNN can thus be divided into two categories, depending on how much information from the forward pass is needed to compute the backward pass. In eventdriven learning, the error is propagated only through spikes [18, 19, 20, 21]. Most notably, EventProp [22] defines exact gradients and can be applied to neuron models without an analytical expression for the postsynaptic potential kernels. Nevertheless, similarly to other existing algorithms, EventProp still requires simulating the network in the forward pass in order to compute postsynaptic events. As these algorithms propagate the error only through spike events, they are prone to fail to converge when the network does not generate enough events to process the signal end-to-end.

The other category that stands in contrast to event-driven learning is RNN-like learning (named after its similarity to nonspiking artificial Recurrent Neural Networks), in which the error information is also propagated through computation time steps which did not elicit a spike [9, 23]. The SuperSpike [24] and SLAYER [25] models are examples of such algorithms. Surrogate gradient methods, commonly used in RNN-like learning, are an alternative approach for overcoming the discontinuous derivative of the spike-generating function [26]. Typically, a standard backpropagation-through-time algorithm [27] is used, as in RNN, with one minor modification: a continuously differentiable function is used in the backward pass as a surrogate of the spike-generation function derivative. Finding the optimal surrogate gradient function is a topic of an ongoing research [28]. Despite achieving a remarkable success in training deep SNN [29, 30], surrogate gradient methods represent an even further departure

from energy-efficient, biologically-inspired learning.

Recently, there has been some research conducted on single-spike time-to-first-spike SNN that specify learning rules which do not require simulating the network over time [8, 31, 32]. Concretely, [8] trains an SNN with simplistic Integrate-and-Fire (IF) neurons by deriving locally exact gradients of the spike-generating function. A similar idea is explored in [31] where the instantaneous synaptic current kernel function is used instead of an exponentially decaying kernel. Furthermore, [32] applies popular deep learning techniques such as maxpooling and batch normalization to this model type, which alleviates issues with training deeper neural architectures. However, to the best of our knowledge, there has been no research that shows how this model can be applied to actual spike trains rather than single spikes.

In this work we derive an algorithm that extends the aforementioned single-spike time-to-first-spike SNN training rules to neurons observing and generating multiple spike trains. In doing so we not only infer locally exact gradients of the spike-generating function, like the EventProp algorithm does, but also express the entire computation in terms of iteratively computing successive spikes (first, second, third, etc.). The latter property stands in stark contrast to other works which simulate the state of the entire network over a finite time window with a fixed time step.

1.2. An overview of Twitter bot detection

Social bots are automated agents that interact with humans and mimic human behavior [33]. In social media environment, such bots may aggregate contents from various sources, automatically respond to custom queries, or even generate content that satisfies some constraints. However, some bot behavior and intent is purposefully misleading or downright malicious [34].

Bot detection systems can be divided into three categories: crowdsourcing, feature-based classification, and social network analysis. Crowdsourcing techniques rely on the ability of hired human experts and volunteers to manually annotate bots based on their profiles, or on sending survey requests to the users

and analyzing their replies [34]. Feature-based classification aims to automate the process by analyzing user-level features, usually by aggregating data pertaining to the user itself and to their activity [35, 36]. It is also possible to perform unsupervised clustering of users based on the temporal similarity of their activity, regardless of their relationship in the social network [15]. This circumvents the time-consuming and costly process of labeling the data. Additionally, the unsupervised systems do not become outdated when new generations of bots, exhibiting patterns of behavior not present during model training, become more prevalent. However, they treat all unclustered examples as legitimate users, limiting their ability to detect bots exhibiting irregular behavior. The last of the three bot detection categories expands the scope of analysis to operate on a large group of users at once [37, 38]. Similarly to the unsupervised user-level methods, they do not become obsolete due to data drift [37]. However, given that they analyze the actual community structure formed by users, they take more time to process information, making them more difficult to operate at scale [39].

In this work we focus on analyzing user data in terms of tweet and retweet actions as the only information available to the model. A tweet is the original message that can be re-broadcasted (i.e., retweeted) by other users. While it is more common to analyze retweets with group-based methods [40, 41], automated behavior can also be made evident by analyzing user-level patterns of retweet activity [42, 43, 15]. The latter is the approach followed in our study.

2. Methods & algorithms

2.1. Signal propagation in time-to-first-spike SNN

This study focuses on a specific type of SNN that is sensitive to the timing of input events and not their rate. Therefore, let us briefly summarize the model first described by Mostafa [8]. This type of network uses IF neurons with exponentially decaying synaptic current kernels. The membrane voltage of a IF neuron with C presynaptic neuron connections is governed by the differential

equation

$$\frac{dV(t)}{dt} = \sum_{c=1}^{C} w_c i_c(t), \qquad (1)$$

where w_c is the weight associated with the c-th synapse (channel), and $i_c(t)$ is the synaptic current driving signal. Assuming that every presynaptic neuron observes a single event at time t_c , the presynaptic current is

$$i_c(t) = \exp\left(-\frac{t - t_c}{\tau_{\text{syn}}}\right) u(t - t_c),$$
 (2)

with τ_{syn} being the synaptic current time constant and u(t) being the step function. The solution to the system of equations defined by (1) and (2) is given by

$$V(t) = V_0 + \tau_{\text{syn}} \sum_{c=1}^{C} w_c \left[1 - \exp\left(-\frac{t - t_c}{\tau_{\text{syn}}}\right) \right] u(t - t_c), \qquad (3)$$

where $V_0=V(0)$ is the initial membrane voltage. The neuron is said to fire at time $t_{\rm out}$ if the voltage exceeds a threshold $V_{\rm thr}$, i.e., $t_{\rm out}=\arg\min_t V(t)\geq V_{thr}$, after which the IF neuron becomes unresponsive to input signals for some time, called the refractory period $\tau_{\rm ref}$. Once the refractory period subsides, the voltage is reset to zero and the summation over impulses in (3) can resume. For now let us consider the case $\tau_{\rm ref}\to\infty$, meaning that the neuron is unable to respond to new inputs following output spike generation. This is an implicit assumption in single-spike SNN [8, 31, 32].

Assuming without the loss of generality $V_0 = 0$ and that there exists a subset of input spikes that cause the postsynaptic neuron to fire

$$Q = \{c : t_c < t_{\text{out}}\},\tag{4}$$

i.e. the $causal\ set$ of input spikes, the solution for $t_{
m out}$ is given in the implicit form

$$z_{\text{out}} = \frac{\sum_{c \in Q} w_c z_c}{\sum_{c \in Q} w_c - \frac{V_{\text{thr}}}{\tau_{\text{syn}}}},$$
 (5)

where

$$z_c(t) = \exp\left(\frac{t_c}{\tau_{\text{syn}}}\right), \ z_{\text{out}}(t) = \exp\left(\frac{t_{\text{out}}}{\tau_{\text{syn}}}\right).$$
 (6)

For completeness we assign $z_{\rm out} = \infty$ when $Q = \varnothing$. A necessary condition for the postsynaptic neuron to fire is that the sum of weights of the causal set of neurons be strictly larger than the scaled threshold voltage [8], i.e., that

$$1 \le z_{\rm out} < \infty \iff \sum_{c \in Q} w_c > \frac{V_{\rm thr}}{\tau_{\rm syn}} \,.$$
 (7)

Note that the condition in (7) assures that the right-hand side of (5) is positive. The formula (5) is differentiable with respect to transformed input spike times $\{z_c\}$ and synaptic weights $\{w_c\}$ with partial derivatives

$$\frac{\partial z_{\text{out}}}{\partial z_c} = \begin{cases} \frac{w_c}{\sum_{c \in Q} w_c - \frac{V_{\text{thr}}}{\tau_{\text{syn}}}} & \text{if } c \in Q\\ 0 & \text{otherwise} \end{cases},$$
(8)

$$\frac{\partial z_{\text{out}}}{\partial w_c} = \begin{cases}
\frac{z_c - z_{\text{out}}}{\sum_{c \in Q} w_c - \frac{V_{\text{thr}}}{r_{\text{syn}}}} & \text{if } c \in Q \\
0 & \text{otherwise}
\end{cases},$$
(9)

therefore it can be used to train a spiking network using the backpropagation algorithm.

2.2. Multiple-input, multiple-output (MIMO) SNN

The model summarized in the previous Section is a time-coding single-spike SNN, unable to process information changing over time. It assumes that every neuron in the model, including input neurons, can elicit at most one spike (by implicitly setting $\tau_{\rm ref} = \infty$). Our goal is to extend the signal propagation rules of the aforementioned model so that its hidden and output neurons are also able to produce multiple spikes each. For brevity, we use a MIMO network descriptor throughout this Section to refer to the model that supports signal propagation with multiple inputs and multiple outputs. In case of multiple events arriving at the input synapse, the equation (1) becomes

$$\frac{dV(t)}{dt} = \sum_{c=1}^{C} w_c \sum_{j=1}^{T_c} i_c^{[j]}(t) = \sum_{c=1}^{C} \sum_{j=1}^{T_c} w_c^{[j]} i_c^{[j]}(t), \qquad (10)$$

where T_c is the number of events observed in channel c. Note that this formula explicitly highlights the fact that every event $t_c^{[j]}$ of channel c is associated with

the same weight $\{j: w_c^{[j]} = w_c\}$. Therefore, a single channel with T_c events is equivalent to T_c virtual (or time-flattened) channels with a single event each. Introducing a new index $\{k: k = 1, ..., K\}$ over these virtual input channels such that $K = \sum_{c=1}^{C} T_c$ we obtain the following representation of (10)

$$\frac{dV(t)}{dt} = \sum_{k=1}^{K} w_k i_k(t) \tag{11}$$

which is identical to (1). It follows that the equations for forward and backward signal propagation through the network introduced in (5)-(9) still hold for the layer observing inputs spiking over time, provided that the indices are substituted where appropriate. The proposed idea of time-flattening the input signal and projecting input layer weights is presented in Figure 1a.

Furthermore, allowing each neuron to spike more than once requires setting a finite nonnegative refractory period τ_{ref} . In that case the causal set of input spikes (4) becomes

$$Q_{m} = \begin{cases} \{k : t_{k} < t_{\text{out}}^{[m]}\} & \text{if } m = 1\\ \{k : t_{\text{out}}^{[m-1]} + \tau_{\text{ref}} < t_{k} < t_{\text{out}}^{[m]}\} & \text{otherwise} \end{cases}$$
(12)

where $\{m: m=1,\ldots,M\}$ is the index over the sequence of neuron output spikes. Computing the m-th output spike time can be done iteratively, noting that M is at most equal to K (the neuron cannot spike more often than once per input spike). The iterative computation over m can be stopped early when an empty causal set is encountered $(Q_m = \varnothing)$. Taking this new definition of a causal set into consideration, the implicit formula for $t_{\text{out}}^{[m]}$ becomes

$$z_{\text{out}}^{[m]} = \frac{\sum_{k \in Q_m} w_k z_k}{\sum_{k \in Q_m} w_k - \frac{V_{\text{thr}}}{\tau_{\text{syn}}}},$$
(13)

whereas the partial derivatives are

$$\frac{\partial z_{\text{out}}^{[m]}}{\partial z_k} = \begin{cases} \frac{w_k}{\sum_{k \in Q_m} w_k - \frac{V_{\text{thr}}}{\tau_{\text{syn}}}} & \text{if } k \in Q_m \\ 0 & \text{otherwise} \end{cases},$$
(14)

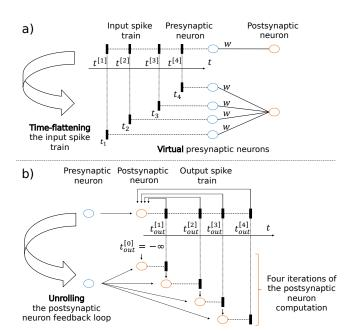


Figure 1: Signal propagation rules in MIMO SNN. The flow of time is represented by an axis going from left to right, i.e., the earliest spike is at the left side of each subfigure. a) A presynaptic neuron that observes multiple input spikes can be represented as multiple virtual presynaptic neurons, each observing a single spike. All virtual presynaptic neurons have the same weight between them and the postsynaptic neuron, identical to the weight associated with the original connection before time-flattening. b) The ability of the postsynaptic neuron to produce spikes depends on all input spike trains from presynaptic neurons, as well as the previously generated output. This feedback loop imposed by the spike causality principle can be unrolled over time, where the postsynaptic neuron computation is repeated with the same input spike trains, but for different timestamps of the previously generated event. This cascade proceeds until it is impossible for the postsynaptic neuron to generate an output spike. The implicit output spike at $t_{\rm out}^{[0]} = -\infty$ designates the initial state of the postsynaptic neuron, i.e., it has not generated a spike yet.

$$\frac{\partial z_{\text{out}}^{[m]}}{\partial w_k} = \begin{cases} \frac{z_k - z_{\text{out}}^{[m]}}{\sum_{k \in Q_m} w_k - \frac{V_{\text{thr}}}{\tau_{\text{syn}}}} & \text{if } k \in Q_m \\ 0 & \text{otherwise} \end{cases},$$
(15)

and additionally

$$\frac{\partial z_{\text{out}}^{[m]}}{\partial w_c} = \sum_{\{k: \ w_k \triangleq w_c\}} \frac{\partial z_{\text{out}}^{[m]}}{\partial w_k} \,, \tag{16}$$

where the set $\{k: w_k \triangleq w_c\}$ denotes the subset of all k for which the virtual (time-flattened) weight w_k corresponds to the original w_c . Note the absence of any explicit dependence between two consecutive output spikes $\{t_{\text{out}}^{[m]}, t_{\text{out}}^{[m+1]}\}$ in equations (13)-(16), or equivalently $\forall_m \partial z_{\text{out}}^{[m+1]}/\partial z_{\text{out}}^{[m]} = 0$. This is fundamentally different from signal propagation in the backpropagation-through-time algorithm [27], and is a direct result of the IF neuron's independence on its own history (i.e., it is memoryless). Instead, the gradients are simply summed over output spikes. This concept of iterating over the M output spikes is summarized in Figure 1b. Signal propagation through the MIMO SNN model can be visualized using a spike raster plot, such as the in Figure 2.

Overall, the proposed algorithm shows how to simulate and train a time-coding MIMO SNN by time-flattening the presynaptic spike trains and unrolling the postsynaptic neuron feedback loop imposed by the spike causality principle. This procedure is sufficient to encode and process information with multiple spikes. However, it must be stressed that the concepts described above and illustrated in Figure 1 specifically refer to operating the model on conventional hardware. Once trained, the spiking network (i.e, synaptic weights and neuron-specific hyperparameters) can be realized on existing neuromorphic hardware, in which case the virtual presynaptic neurons are no longer needed (hence the name) as reusing neurons for multiple input and output events is implied.

2.3. MIMO SNN loss function

The original model proposed by [8] was trained using a loss function with two components. The first one is a modification of the cross-entropy loss with

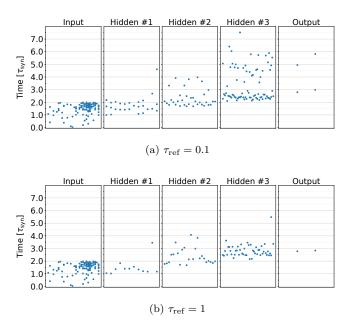


Figure 2: Spike raster plot for models trained with two different values of $\tau_{\rm ref}$ responding to the same input example.

softmax normalization

$$L(z,y) = -\sum_{p=1}^{P} y_p \ln \left(\frac{\exp(-z_p)}{\sum_{p=1}^{P} \exp(-z_p)} \right),$$
 (17)

where:

- \bullet P the number of output channels,
- y_p a binary indicator (0 or 1) of the desired output channel p spiking first,
- z_p the transformed spike time of the p-th output channel.

This loss function encourages the model to use rank-order coding [44] to represent the output, without explicitly specifying the time of each spike. The second component of the loss function is a spike regularization term, which promotes network spiking activity by ensuring a nonnegative denominator of (5)

$$R_{\text{spiking}} = \sum_{h=1}^{H} R_h \,, \tag{18}$$

where $R_h = \max \left(0, V_{\text{thr}}/\tau_{\text{syn}} - \sum_{c=1}^{C_h} w_{ch}\right)$ and the index h runs over all neurons in the network H. The overall loss function minimized by the model is

$$L_{\text{total}}(z,y) = \frac{1}{N} \sum_{n=1}^{N} L_n(z,y) + \gamma R_{\text{spiking}}, \qquad (19)$$

where $L_n(z, y)$ is the cross-entropy loss (17) for the *n*-th example of the batch of size N, and γ is a hyperparameter.

We posit that the penalty term should be applied only when "the task is not solved". For classification models this entails that the output of the network is different from the expected ground truth. Such approach would result in models that are more efficient in terms of the number of spikes needed to propagate the signal through the network, compared to the original approach (which makes all neurons in the network produce at least one spike). The proposed heuristic is thus

$$R_{\text{spiking}}^* = \frac{1}{\sum_{n=1}^{N} \mathbf{1} (y_n \neq \hat{y}_n)} \sum_{n=1}^{N} \mathbf{1} (y_n \neq \hat{y}_n) R_{\text{spiking}}^{[n]},$$
 (20)

where n runs over all examples withing a training minibatch N; $R_{\text{spiking}}^{[n]}$ is the spike-firing penalty term in (18), and $\mathbf{1}(A)$ is the indicator function. The argument of the indicator function is a short-hand notation for the output of the network \hat{y}_n being different from the expected ground truth y_n . The proposed heuristic (20) dynamically scales the spike-firing penalty term during training it acts as a mean penalty over the minibatch examples if the network returns an incorrect output for all examples, and it assigns an increasingly larger weight to each incorrectly predicted example as the training progresses. For completeness

$$R_{\text{spiking}}^* = 0$$
 if $\bigvee_{n \in \{1,\dots,N\}} \mathbf{1} (y_n \neq \hat{y}_n) = 0$.

Furthermore, some adjustments to the loss function components are necessary in order to use them in a MIMO SNN context, particularly to the spike regularization term. The formula (18) can be trivially extended to networks with inputs spiking over time by substituting the index over the input neurons c with an index over virtual input channels k. We can also apply regularization to each

neuron output spike m separately. Thus, the regularization term that considers the MIMO SNN signal propagation rules is

$$R_{\text{spiking}} = \sum_{h=1}^{H} \sum_{m=1}^{M_h} R_h , \qquad (21)$$

where R_h is redefined as $R_h = \max\left(0, V_{\text{thr}}/\tau_{\text{syn}} - \sum_{k=1}^{K_h} w_{kh}\right)$. However, this implicitly assumes that every presynaptic weight w_{kh} is associated with an event t_{kh} . We have previously shown [45] that this need not be the case as SNN can exhibit a sparse neuron activity. It is entirely possible that for some neuron h the inequality $\sum_{k=1}^{K_h} w_{kh} > V_{\text{thr}}/\tau_{\text{syn}}$ holds and yet the neurons does not fire anyway. This scenario might occur if none of the presynaptic neurons observe an event. Therefore, (21) can be reformulated to make this dependence on input spikes explicit

$$R_{\text{spiking}} = \sum_{h=1}^{H} \sum_{m=1}^{M_h} R_{mh},$$
 (22)

where $R_{mh} = \max \left(0, V_{\text{thr}}/\tau_{\text{syn}} - \sum_{k \in B_{mh}} w_{kh}\right)$ with $B_{mh} \subset Q_{mh}$ being the set of valid inputs for the m-th output of the n-th postsynaptic neuron

$$B_{mh} = \begin{cases} \{k : t_{kh} < \infty\} & \text{if } m = 1\\ \{k : t_{\text{out}_h}^{[m-1]} + \tau_{\text{ref}} < t_{kh} < \infty\} & \text{otherwise} \end{cases}$$
 (23)

For completeness

$$R_{mh} = 0$$
 if $\{k : t_{kh} < \infty\} = \emptyset$.

In our preliminary experiments we found that the penalty term is too strong for m > 1, skewing the training objective towards forcing neurons to output multiple spikes, rather than letting it focus on solving the actual task. As such, we train our models by setting $\forall_{m>1} R_{hm} = 0$, which only penalizes neurons that do not spike at all (alternatively one might consider applying a smaller weight to subsequent spikes).

On another note, the modified cross-entropy loss as defined by (17) ignores the fact that each output layer neuron can produce multiple spikes. This means that for the last layer, either the refractory period could be set to $\tau_{\rm ref} = \infty$, or that all m > 1 output spikes could simply be ignored (as they have no impact on the gradient propagation anyway). Both approaches lead to the same result.

Applying the dynamic scaling factor (20) to the spike regularization term computed over the set of valid inputs (22), and plugging the result into the loss function minimized by the original model (19) leads to the following loss function minimized by the MIMO SNN training objective

$$L_{\text{total}}(z, y) = \frac{1}{N} \sum_{n=1}^{N} L_n(z, y) + \gamma \frac{1}{\sum_{n=1}^{N} \mathbf{1} (y_n \neq \hat{y}_n)} \sum_{n=1}^{N} \mathbf{1} (y_n \neq \hat{y}_n) R_{\text{spiking}}^{[n]}.$$
 (24)

3. Experimental setup

3.1. Dataset description

The RT_{BUST} study reported in [15] used Twitter Premium Search API to compile a list of all Italian retweets shared between 18 June 2018 and 1 July 2018. In this 2-week period there have been almost 10M retweets shared by 1.4M distinct users. The compiled dataset¹ consists of records of retweet timestamps associated with some original tweets. These records can be aggregated based on user id such that each user is characterized by a different number of tweet-retweet pairs. Importantly, the dataset contains no information on the content of shared tweets, thus the goal is to classify legitimate and bot users based solely on retweet timestamps. To supplement this vast collection of unlabeled records, about 1000 accounts were manually annotated based on published annotation guidelines for datasets containing social bots [34].

We limit the scope of our analysis to the labeled portion of this dataset and, in contrast to the original study, apply a supervised learning algorithm on

¹The dataset is available at https://doi.org/10.5281/zenodo.2653137

individual data points. Let us introduce a retweet delay as a difference between retweet and the origin-tweet timestamps, expressed in minutes. This quantity can be treated as describing an observed event, hence we denote it as t in order to avoid introducing additional notation. We filter the records so that only those with both tweet and retweet timestamps occurring from 18 June 2018 to 1 July 2018 (exclusive) are kept, meaning that the retweet delay attribute is bounded from above to about $\tau_{\rm max} = 2 \cdot 10^4$ minutes (2 weeks) ². Additionally, only records with a delay of at least $\tau_{\rm min} = 10^{-1}$ minutes were considered for further analysis. Records with a retweet delay below the selected $\tau_{\rm min}$ can be considered a sign of either auto-retweeting bots, or legitimate users that were refreshing their feed as the tweet was posted and decided to retweet immediately. Either way, in our opinion, this does constitute a typical user behavior. As a result of this filtering step, 11.73% of all records were removed.

Finally, the records were grouped by the retweeting user and by label. This allowed us to construct a set of data points X with elements $x = [t_1, \dots, t_U; U]$ such that $\tau_{\min} < t_1 < \dots < t_U < \tau_{\max}$ are the retweet delays bounded by observation time τ_{\max} and $U = U(\tau_{\max})$ is the length of the sequence. We obtain a nearly balanced data subset with 366 examples of legitimate users and 389 examples of bot users. These user tweet-retweet sequences have, on average, about 113 events with a maximum of 698. The remaining 46,883 cases are unlabeled and were not used in this study.

3.2. Signal preprocessing

The tweet-retweet sequences obtained in the previous Section are characterized by two peculiar traits that make designing an SNN-based classifier difficult. First, we note that all events occur in only one channel. If all neurons in the network have the same value of parameters $\tau_{\rm syn}$, $\tau_{\rm ref}$ and $V_{\rm thr}$, then this scenario imposes additional constraints on the weights during training. First of all, the

 $^{^2}$ Throughout the rest of this paper, we express all units of time in terms of minutes, same as the original RT_{BUST} study.

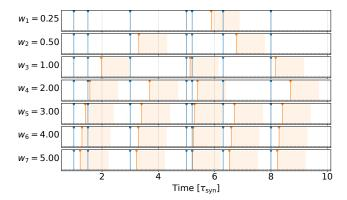


Figure 3: Simulated spike trains from a simple network with one input neuron and seven postsynaptic neurons. In blue: input spike train (the same in all rows), in orange: spikes generated by postsynaptic neurons. The shaded area denotes the refractory period after generating a spike. All output neurons have the same values of parameters $\tau_{\rm syn}$, $\tau_{\rm ref}$ and $V_{\rm thr}$ with the only difference between them being the synaptic weight w. Note that if the weight it too large (in this case $w \geq 3$), the neuron elicits a spike in response to every input event, unless it occurs during the refractory period, effectively repeating the input sequence. This means that a group of postsynaptic neurons is redundant because they produce almost identical spike trains. In such scenario, output sequence variability could be improved by adjusting the values of $\tau_{\rm syn}$, $\tau_{\rm ref}$ and $V_{\rm thr}$ for each neuron individually.

synaptic weight of each connection must be positive, otherwise the postsynaptic neuron is unable to produce any spike. This also means that each postsynaptic neuron eventually produces a spike as IF neurons are unable to lose charge if all presynaptic weights are positive. Additionally, if some weights are too large, then it is possible that the associated postsynaptic neurons will produce nearly identical spike trains, with only slight variations in spike frequency and their timing (illustrated in Figure 3). While it is certainly not impossible to train a network with such constraints on the input layer, we can expect this to be more difficult. In fact, in Section 4.3 we empirically show that training a model with a single input neuron is indeed more challenging than the alternative.

For these reasons we explored the possibility of transforming input spike trains into multiple sequences of fewer events. This is analogous to conducting feature engineering instead of relying on trainable feature extractors in artificial

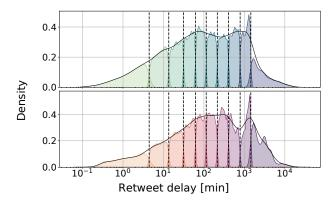


Figure 4: The result of binning the empirical density functions of the two classes (above - legitimate users; below - bots) into 10 bins over a given data split.

neural networks. Loosely inspired by the technique of binning used in neuroscientific studies, we identify a collection of bins that divide the spike train aggregated over all examples into sub-sequences with approximately the same number of events in each bin³. This concept is illustrated in Figure 4 by dividing the empirical density functions of the two classes. Importantly, the step that identifies binning thresholds is computed over the training examples. Each sub-sequence can then be shifted so that it starts at t = 0 by subtracting the corresponding binning threshold.

We note that binning is a valid strategy for this specific problem because it is assumed that events aggregated into a tweet-retweet sequence of each user are independent of one another [15]. While this is a reasonable assumption given the data, in reality it seems plausible that graph community structure and programmed bot behavior play an important role in what gets retweeted, and when. Additionally, the IF neuron exhibits the memoryless property where the internal state of the neuron (membrane voltage) is preserved regardless of how recent was the previous event. Finally, as a side note, taking the binning approach to the extreme would result in a multitude of thin bins such that there

³By contrast, in neuroscience binning produces the number (or an average number of) events that had occurred in a given time interval over multiple repetitions of the experiment.

is at most one event per bin for each example. We did not consider this to be worth pursuing as it would greatly increase the number of neurons needed to represent the signal in the input layer of the network.

The second point that needs to be addressed is that events occur at timescales differing by almost five orders of magnitude. At such scales the transformed events in (6) easily surpass the limits of double-precision floating-point data format. This problem still persists even after binning the sequences and shifting each sub-sequence so that it has a common starting time of t = 0. It is easy to see (Figure 4) that for bins with a higher index, the range of event times, while reduced, is still relatively large for the network. And so, we can either increase the number of bins (but as discussed previously this does not seem to be a suitable approach), or transform each sequence to reduce the range of observed values. Therefore, we apply a log-transform to binned sub-sequences with events occurring in range $t \in [T_{c-1}, T_c)$ such that

$$\forall_{t \in [T_{c-1}, T_c)} \ g(t; b_c, c) = \log_{b_c} (t - T_{c-1} + 1)$$
 (25)

for $b_c > 1$, where $c \in \{1, 2, \ldots\}$ is the index of the bin, T_c is the upper boundary of the c-th bin (i.e., the threshold), and $T_0 = 0$. Each bin corresponds to a single network input channel, hence we reuse the index c to make this explicit and avoid introducing additional notation. Note that each transformed sequence is shifted to start at t = 0. This transform is controlled by a single parameter b_c , the base of the logarithm. Note that $g(t; b_c, c)$ is a decreasing function of b_c .

In general, the transform in (25) allows setting a different b_c for each bin (channel). In our experimental scope we consider two strategies for selecting b_c :

1. Setting the same base b > 1 for all bins

$$\forall_{t \in [T_{c-1}, T_c)} \ g_1(t; b, c) = \log_b \left(t - T_{c-1} + 1 \right) . \tag{26}$$

2. Adjusting the base of the logarithm for each bin separately so that all bins have the same range of values after transform

$$g_2(t; \kappa, c) = \frac{\kappa}{g_1(T_c; b, c)} g_1(t; b, c),$$
 (27)

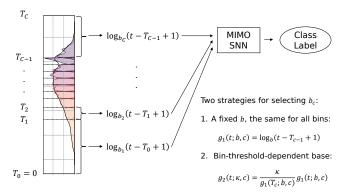


Figure 5: A diagram of the preprocessing steps to obtain signals used to train a MIMO SNN on Twitter dataset.

where κ is the time-instant assigned to the threshold T_c after transform, i.e., $\kappa = g_2(T_c; \kappa, c)$. Note that in this strategy the value of the parameter b does not matter as the actual logarithm base for a given bin c is controlled by the boundaries T_{c-1} , T_c and the parameter κ . For simplicity, we use the same κ for all bins.

The difference between these two approaches lies in the range of values produced by the transform. Strategy $g_1(t;b,c)$ is unbounded from above and so it might be difficult to select a single b that works at both short and long timescales. Conversely, the function $g_2(t;\kappa,c)$ squeezes all values to lie in the range $[0,\kappa]$, which might make it easier for the network to learn the relationship between events at different timescales.

Figure 5 summarizes the outlined preprocessing steps. We found that applying the *b*-parameterized log-transform on binned sub-sequences sufficiently addressed our concerns for training the proposed spiking neural network. Note that while the log-transform (25) has the unfortunate effect of significantly increasing the latency of the model, we are only interested in the final classification prediction of the model and not its real-time performance.

4. Results & discussion

In all of our experiments we used the same C-12-24-48-2 architecture, where C is the number of bins used to preprocess the spike train, the network has 2 output neurons, and other digits represent the number of neurons in the hidden layers. This produces a relatively small network of about 1536 + 12C parameters. However, a MIMO SNN model complexity is not only determined by the number of parameters, but also by the refractory period $\tau_{\rm ref}$ (see (12)) which controls how often each neuron in the network is able to spike.

4.1. The impact of the refractory period on signal propagation

In order to settle on a single value of $\tau_{\rm ref}$ to use in our experiments, we conducted a preliminary study by training the classification model on a small subset of data (stratified random 10% sample). We considered $\tau_{\rm ref} \in [0.01, 1]$, selected on a 5-point logarithmically-spaced grid. The data was preprocessed into 30 bins, with bin-threshold-dependent logarithm base b_c computed for $\kappa = 3$. All models were trained for 200 epochs of 10 update steps each, with a batch size of 64. This was enough to reach perfect classification score on the training set for each model (note that in this experiment we were not interested in the classifier's performance on unseen data, but rather in how the signal propagates through the MIMO network). The synaptic regularization parameter was set to $\gamma = 10^5$ in order to promote spiking activity in the network. Training was repeated 5 times in order to average-out processing time measurements.

In the preliminary study we measured the average time it took to finish the training epoch, as well as sparsity-adjusted average number of spikes produced by the network in response to input signals. The "sparsity-adjusted" term states that only the active (i.e., not quiescent) neurons are considered when discussing the impact of the choice of $\tau_{\rm ref}$. To succinctly describe this measure we introduce the network activity indicator

$$NAI = \frac{1}{N \sum_{l=1}^{L} H_l} \sum_{n=1}^{N} \sum_{\ell=1}^{L} \sum_{h_{\ell}=1}^{H_{\ell}} M_{nh_{\ell}}, \qquad (28)$$

where $M_{nh_{\ell}}$ is the number of output spikes generated by the h_{ℓ} -th neuron of the ℓ -th layer in response to the n-th example in the minibatch.

The results are summarized in Figure 6. We observe that both the NAI measure and the epoch training time rapidly increase in the initial stages (the first 50 epochs) because then the spike regularization term forces the model to learn how to propagate the signal through the network. Afterwards, the training time remains relatively constant throughout the rest of the training, while NAI continues to increase, albeit at a much slower rate. Note that the growth of NAI over training epochs is unbounded because there is no term in the loss function (24) that encourages the network to generate fewer spikes. This shows that setting a smaller $\tau_{\rm ref}$ causes the network to produce more spikes.

Surprisingly, however, the obtained processing time measurements do not support the notion that it is possible to predict which model will take the least amount of time to process the examples based solely on the value of the refractory period. Such relationship was anticipated as the number of iterations needed to compute all output spikes in (13) increases as $\tau_{\rm ref}$ decreases. Perhaps repeating this experiment significantly more times would allow us to reach a conclusive answer as processing time measurements are notoriously unreliable. Nevertheless, normalizing the processing time measurements separately for each experimental run shows that the relative increase in processing time over the training epochs is similar across different scenarios. Based on all these results, we settle on $\tau_{\rm ref} = 0.1$ in our further experiments as the largest $\tau_{\rm ref}$ that still exhibits a steep increase in NAI measure over training steps.

4.2. Bot detection - binary classifier performance

In our experiments on the classification problem, having fixed the value of $\tau_{\rm ref}$, we explored the impact of proposed preprocessing on model performance. We constructed a grid over preprocessing parameter space, selecting the number of bins from the set $C \in \{10, 20, 30, 40, 50\}$, whereas the log-transform parameter was set to either $b_c(\kappa)$ for $\kappa \in \{1, 2, 3\}$, or $b \in \{10, 30\}$. For every pair of parameters on this grid, several models were trained and evaluated with 5-fold

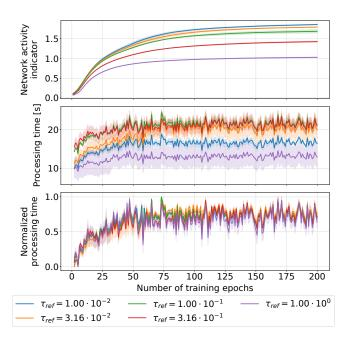


Figure 6: The impact of the refractory period $\tau_{\rm ref}$ on a trained MIMO SNN properties. Top panel: sparsity-adjusted average number of spikes produced by the network. Middle panel: average epoch training time. Bottom panel: normalized average epoch training time.

cross validation. Thus, in total 125 models were trained. All models were trained for 50 epochs, each with 100 training steps over 64 class-balanced training examples. The learning rate was set to 10^{-3} in all steps. The synaptic regularization term factor γ varied substantially depending on the current training epoch—initially set to 10^5 in order to guide the model towards a state in which it is able to propagate spikes throughout all layers. After 10 epochs, we set $\gamma = 10^{-2}$ so that the model could focus on minimizing the task-specific loss term (17).

Given the small dataset size (366 legitimate users and 389 bots), we opt to use data augmentation in order to increase the effective training split size. Two types of augmentation were used:

- drop events with probability 0.1,
- randomly shift each event in time by t_{δ} uniformly distributed in (-0.05, 0.05), independently with probability 0.3.

The latter augmentation type is applied only after the sequence has been preprocessed, making sure that the shift-augmented sub-sequence is still composed of events occurring at nonnegative time.

The classification accuracy achieved by all models trained over the preprocessing grid is summarized in Table 1. The results obtained during the hyperparameter search on the preprocessing grid do not suggest an existence of some pattern that holds across different number of bins or the transform choice. Notably, however, the setting denoted by the parameter b=30 seems to be more robust compared to other settings in that it is the only one that allowed the model to consistently reach an accuracy over 70% regardless of the number of bins.

Overall, the wide range of performance classification scores reported by different models suggest that it is imperative to perform hyperparameter tuning when using the proposed MIMO network for this specific scenario of extremely long-range dependencies between events. Nevertheless, it must be stressed that the hyperparameters associated with the neural model itself ($V_{\rm thr}$, $\tau_{\rm syn}$, $\tau_{\rm ref}$) can be selected heuristically. Firstly, note that $V_{\rm thr}$ only influences the scale of trained weights and has no impact on training dynamics, making the choice of $V_{\rm thr}$ arbitrary. On the other hand, the time constants $\tau_{\rm syn}$ and $\tau_{\rm ref}$ can be selected according to the input event distribution. The post-synaptic potential constant $\tau_{\rm syn}$ needs to be longer than the relevant temporal patterns present in the input data [16]. Lastly, setting $\tau_{\rm ref} < \tau_{\rm syn}$ prevents the scenario in which the network rarely generates events.

Table 2 compares our best model with the results obtained in the original study [15] in terms of accuracy, recall, precision, F_1 -score and Matthews correlation coefficient (MCC). Our MIMO SNN model outperforms all of the presented supervised approaches (Botometer, Social fingerprinting), as well as most of the unsupervised methods (HoloScope; PCA- and TICA-based RT_{BUST}). Importantly, the latter group of methods relied on fitting the model on the entire unlabeled dataset of 63,762 accounts and evaluating on the labeled portion, whereas we focus only on the annotated subset (as outlined in Section 3.1),

Table 1: Classification accuracy for MIMO SNN models trained on Twitter tweet-retweet dataset, depending on the chosen preprocessing parameters. A star (\star) denotes the best result for a row, whereas the diamond (\diamond) denotes the best result in a column.

[
Stratified 5-fold		Log-transform-related parameter							
cross validation		b = 10	b = 30	$b_C(\kappa=1)$	$b_C(\kappa=2)$	$b_{\mathcal{C}}(\kappa = 3)$			
Number of bins	C = 10	*\$73.25 ± 3.71	70.33 ± 3.83	68.74 ± 3.09	68.08 ± 4.20	68.61 ± 10.46			
	C = 20	70.20 ± 3.72	*70.60 ± 1.65	67.95 ± 2.70	70.33 ± 3.80	68.21 ± 5.70			
	C = 30	67.42 ± 2.03	*\$71.52 ± 4.74	69.40 ± 4.76	70.86 ± 1.83	69.14 ± 3.09			
	C = 40	69.27 ± 2.67	70.60 ± 4.40	66.75 ± 4.50	69.40 ± 4.42	*\$71.13 ± 3.49			
	C = 50	67.68 ± 4.20	71.26 ± 6.22	*\$72.19 ± 3.82	♦70.99 ± 4.26	68.08 ± 3.61			

composed of about 755 labeled cases in total. We note that the Variational Autoencoder (VAE) variant of the RT_{BUST} model performed better than our approach. As this model also leveraged the unlabeled portion of the dataset, it stands to reason that there is a clear benefit to clustering-based methods, in which the presence of a suspicious behavior emerges only when analyzing user in groups, rather then as individuals. Furthermore, we note that the examples examined in [15] were manually labeled and thus any incorrectly labeled cases could have had a much bigger impact on the supervised model trained with significantly fewer examples. Lastly, it is important to note that the original study lacks technical details related to the LSTM-VAE network architecture, which prevents us from making a comparison between the two methods that is adjusted for model complexity as expressed by the number of trainable parameters.

4.3. Model ablation study

For the best-performing model, we ran an ablation study experiment in order to determine which components of the proposed approach have a significant impact on model performance. We tested four scenarios:

- 1. no data augmentation,
- 2. setting $\tau_{\rm ref} = \infty$, i.e., preventing the neurons in the network from spiking more than once in response to a given input signal,

Table 2: Comparison of model performance on the bot detection task between different techniques.

	Technique	Accuracy	Recall	Precision	F ₁ -score	MCC
	Botometer	58.30	30.98	69.51	42.86	0.2051
[15]	HoloScope	49.08	0.49	28.57	0.96	-0.0410
	Social fingerprinting	71.14	89.78	65.62	75.82	0.4536
	RT _{BUST} (PCA)	51.54	95.12	51.11	66.49	0.0446
[15]	RT _{BUST} (TICA)	53.64	95.12	52.28	67.47	0.1168
	RT _{BUST} (VAE)	87.55	81.46	93.04	86.87	0.7572
our	MIMO SNN	73.25 ± 3.71	69.56 ± 8.93	76.39 ± 3.34	72.46 ± 5.08	0.47 ± 0.07

- 3. no splitting of channels into separate bins,
- 4. no log transform.

Each one represents a single change to the experimental protocol outlined in Section 4.2. Clearly, with the exception of the first scenario, these changes have a major impact on how the signal is propagated through the network or on training dynamics.

As evidenced in Table 3, removing any of the components causes a reduction in model performance. This shows that the proposed data augmentation scheme was effective in mitigating the problem of overfitting. Furthermore, the drop in performance for the $\tau_{\rm ref} = \infty$ scenario suggests that some of the model's capacity to process information is tied to the ability to process it over time. Unsurprisingly, not splitting the input spike train into multiple bins makes it more difficult for the model to learn long range dependencies, which is an effect that was anticipated while designing this preprocessing step. Lastly, the sharpest drop in performance is observed when the data is passed through the network without any transform that squashes the range of values at its input. Note that the obtained average accuracy of 47.68% is quite close to the ratio of the number of legitimate users to all users in the stratified evaluation data split (48.48%). This means that the model was unable to learn anything, most likely because using raw event times as large as $2 \cdot 10^4$ minutes transformed according to (6) surpasses the limits of double-precision floating-point data for-

Table 3: Model performance in the ablation study, given the specified scenario.

Scenario	Accuracy	Recall	Precision	F ₁ -score	мсс
baseline	73.25 ± 3.71	69.56 ± 8.93	76.39 ± 3.34	72.46 ± 5.08	0.47 ± 0.07
no data augmentation	66.89 ± 1.45	58.09 ± 10.61	73.77 ± 6.50	63.80 ± 5.60	0.36 ± 0.03
infinite refractory period	67.28 ± 2.64	56.30 ± 4.52	74.44 ± 5.63	63.89 ± 3.06	0.36 ± 0.06
no channel-splitting	63.18 ± 4.60	69.67 ± 14.22	62.61 ± 2.74	65.42 ± 7.49	0.27 ± 0.10
no log transform	47.68 ± 1.18	0.00 ± 0.00	0.00 ± 0.00	0.00 ± 0.00	-0.06 ± 0.07

mat, making training impossible. Note that the trained models are in general biased towards higher precision, with the exception of the channel-splitting scenario, despite being trained with a nearly class-balanced data. In bot-detection scenarios it is preferable to favor precision instead of recall as the system administrator should be reasonably certain that a user is a bot before taking action.

For completeness, Figure 7 shows representative examples of confusion matrices for the five scenarios, chosen according to the MCC. It is evident in the results for the experiment without log transform that for a failed model all predictions are towards the negative class. This stems from the assumption that if the output layer produces no events, then the model should return the negative class prediction. However, this effect is negligible for properly trained models—in other scenarios less than 1% of bot accounts were misclassified as legitimate users due to this assumption.

4.4. Computational complexity of the MIMO SNN

Let us briefly comment on the computational burden of the MIMO SNN in general, without the preprocessing steps that are specific to the Twitter dataset. The proposed algorithm slightly increases the complexity of the single-spike version proposed in [8]. Note that it is possible to compute the first output spike of all output neurons in a given layer observing numerous minibatch input examples presented to presynaptic neurons in a single pass through the layer (see [32] for a simplified version of this algorithm). While the proposed MIMO SNN approach introduces an unavoidable feedback loop resulting from the spike causality principle, it does not prevent the model from training with

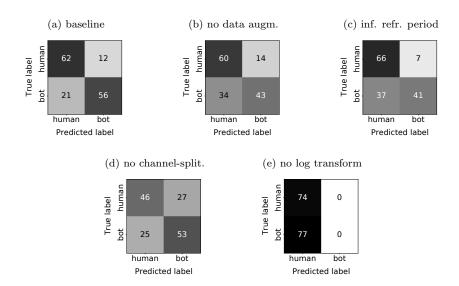


Figure 7: Confusion matrices corresponding to the best-performing iteration with respect to MCC value for five ablation experiment scenarios.

modern deep learning software frameworks. During such iterative search over output spikes, the SNN is no different from a nonspiking RNN.

Note that the proposed algorithm iterates over the space of discrete output spike events rather than discretizing time at a predefined time-resolution. This leads to significantly fewer iterations when computing the full output spike train of each neuron than the alternative requiring a discretized time simulation. Additionally, this allows MIMO SNN to compute arbitrarily late events w.r.t. reference time, whereas discretized-time algorithms are limited in scope by the simulation window. In our experiments we did not impose an upper limit on the number of events generated by a single neuron, relying instead on the exhaustive search over the event space. Note that this event space is finite as each neuron cannot generate more events than it observes across all synapses.

Nevertheless, the MIMO SNN adversely scales with the number of events observed by presynaptic neurons, as well as by those generated by its neurons. The former has the biggest effect on the input layer, in which the number of virtual (time-flattened) channels can be extremely large when the network has

numerous input neurons, each observing lengthy spike trains. This limits the applicability of our approach to multichannel data streams without too many events (although it is difficult to estimate what this upper limit actually is), unless the dataset is preprocessed to contain fewer events. Furthermore, the average processing time increases with the number of spikes generated by the layer as the feedback loop must be unrolled over time. However, note that each successive spike is less likely to be generated (because the causal set shrinks with each iteration), making the computational complexity of subsequent iterations smaller than the preceding one. Fortunately, the network spiking activity can be controlled by the $\tau_{\rm ref}$ hyperparameter, as evidenced by our experiments.

5. Conclusion

This study introduces a MIMO SNN model which extends existing time-coding single-spike time-to-first-spike SNN models by defining the rules for spike propagation throughout the layers when simulating the network on conventional hardware. Once trained, the model can be realized on existing neuromorphic devices that implement the IF neuron computation. In contrast to other works, the proposed MIMO SNN expresses the entire algorithm in terms of iteratively calculating successive spikes, which stands in contrast to other works simulating the state of the entire network over a finite time window with a fixed time step. The proposed MIMO SNN is suited towards datasets with spike trains composed of relatively infrequent events occurring at different timescales, such as the Twitter user activity dataset. Furthermore, the algorithm can be implemented in modern deep learning frameworks, making it scalable to large volumes of data.

The model was applied to a labeled subset of Twitter user activity data in order to determine whether each analyzed user is legitimate or not. Choosing a dataset with a time horizon of a 2-week-period allowed us to show that the model is able to process time series composed of events occurring at timescales differing by almost five orders of magnitude. Our best model achieved an accuracy

score of 73.25%, compared to 87.55% obtained by the original RT_{BUST} study. However, we note that the latter is an unsupervised learning algorithm and is therefore able to infer different non-overlapping patterns of activity of distinct groups of users not present in the class-label-aggregated data. Furthermore, our model relies on about 755 labeled example compared to the 63,762 unlabeled cases used to train RT_{BUST}. As the data was manually labeled by the authors of the study, any incorrectly labeled examples could have had a much bigger impact on the supervised model trained with significantly fewer examples. We have shown that the proposed MIMO SNN operates directly in an event-domain, and so there is no need to encode the time series in any way for it to be processed by the model. In addition to the classification model feasibility study, this work showcased novel signal preprocessing steps, exemplary spike train data augmentation techniques, and the heuristic of modifying regularization scale factor during training to tackle this challenging dataset. We found that these concepts were critical at preventing overfitting and stabilizing the training procedure, as evidenced by the results of the ablation study. We hope to explore these insights in future works.

References

- [1] M. Pfeiffer, T. Pfeil, Deep learning with spiking neurons: Opportunities and challenges, Frontiers in Neuroscience 12 (2018) 774.
- [2] J. K. Eshraghian, M. Ward, E. O. Neftci, X. Wang, G. Lenz, G. Dwivedi, M. Bennamoun, D. S. Jeong, W. D. Lu, Training spiking neural networks using lessons from deep learning, Proceedings of the IEEE 111 (2023) 1016– 1054.
- [3] B. Rueckauer, I.-A. Lungu, Y. Hu, M. Pfeiffer, S.-C. Liu, Conversion of continuous-valued deep networks to efficient event-driven networks for image classification, Frontiers in Neuroscience 11 (2017) 682.
- [4] R. Midya, et al., Artificial neural network (ANN) to spiking neural network

- (SNN) converters based on diffusive memristors, Advanced Electronic Materials 5 (9) (2019) 1900060.
- [5] C. Stöckl, W. Maass, Optimized spiking neurons can classify images with high accuracy through temporal coding with two spikes, Nature Machine Intelligence 3 (3) (2021) 230–238.
- [6] P. Falez, P. Tirilly, I. M. Bilasco, P. Devienne, P. Boulet, Unsupervised visual feature learning with spike-timing-dependent plasticity: How far are we from traditional feature learning approaches?, Pattern Recognition 93 (2019) 418–429.
- [7] M. Mozafari, M. Ganjtabesh, A. Nowzari-Dalini, S. J. Thorpe, T. Masquelier, Bio-inspired digit recognition using reward-modulated spike-timingdependent plasticity in deep convolutional networks, Pattern Recognition 94 (2019) 87–95.
- [8] H. Mostafa, Supervised learning based on temporal coding in spiking neural networks, IEEE Transactions on Neural Networks and Learning Systems 29 (7) (2017) 3227–3235.
- [9] Y. Wu, L. Deng, G. Li, J. Zhu, L. Shi, Spatio-temporal backpropagation for training high-performance spiking neural networks, Frontiers in Neuroscience 12 (2018) 331.
- [10] D. Rasmussen, NengoDL: Combining deep learning and neuromorphic modelling methods, Neuroinformatics 17 (4) (2019) 611–628.
- [11] Y. Guo, W. Peng, Y. Chen, L. Zhang, X. Liu, X. Huang, Z. Ma, Joint A-SNN: Joint training of artificial and spiking neural networks via self-Distillation and weight factorization, Pattern Recognition 142 (2023) 109639.
- [12] G. Orchard, A. Jayawant, G. K. Cohen, N. Thakor, Converting static image datasets to spiking neuromorphic datasets using saccades, Frontiers in Neuroscience (2015).

- [13] E. Doutsi, L. Fillatre, M. Antonini, P. Tsakalides, Dynamic image quantization using leaky integrate-and-fire neurons, IEEE Transactions on Image Processing 30 (2021) 4305–4315.
- [14] A. Javanshir, T. T. Nguyen, M. A. P. Mahmud, A. Z. Kouzani, Advancements in algorithms and neuromorphic hardware for spiking neural networks, Neural Computation 34 (6) (2022) 1289–1328.
- [15] M. Mazza, S. Cresci, M. Avvenuti, W. Quattrociocchi, M. Tesconi, RTbust: Exploiting temporal patterns for botnet detection on Twitter, in: Proceedings of the 10th ACM Conference on Web Science, 2019, pp. 183–192.
- [16] S. M. Bohte, J. N. Kok, H. La Poutre, Error-backpropagation in temporally encoded networks of spiking neurons, Neurocomputing 48 (1-4) (2002) 17– 37.
- [17] J. H. Lee, T. Delbruck, M. Pfeiffer, Training deep spiking neural networks using backpropagation, Frontiers in Neuroscience 10 (2016) 508.
- [18] D. Huh, T. J. Sejnowski, Gradient descent for spiking neural networks, Advances in Neural Information Processing Systems 31 (2018).
- [19] W. Zhang, P. Li, Temporal spike sequence learning via backpropagation for deep spiking neural networks, Advances in Neural Information Processing Systems 33 (2020) 12022–12033.
- [20] N. Perez-Nieves, D. Goodman, Sparse spiking gradient descent, Advances in Neural Information Processing Systems 34 (2021) 11795–11808.
- [21] Y. Zhu, Z. Yu, W. Fang, X. Xie, T. Huang, T. Masquelier, Training spiking neural networks with event-driven backpropagation, Advances in Neural Information Processing Systems 35 (2022) 30528–30541.
- [22] T. C. Wunderlich, C. Pehle, Event-based backpropagation can compute exact gradients for spiking neural networks, Scientific Reports 11 (1) (2021) 12829.

- [23] H. Zheng, Y. Wu, L. Deng, Y. Hu, G. Li, Going deeper with directly-trained larger spiking neural networks, in: Proceedings of the AAAI Conference on Artificial Intelligence, Vol. 35, 2021, pp. 11062–11070.
- [24] F. Zenke, S. Ganguli, SuperSpike: Supervised learning in multilayer spiking neural networks, Neural Computation 30 (6) (2018) 1514–1541.
- [25] S. B. Shrestha, G. Orchard, SLAYER: Spike layer error reassignment in time, Advances in Neural Information Processing Systems 31 (2018) 1419–1428.
- [26] E. O. Neftci, H. Mostafa, F. Zenke, Surrogate gradient learning in spiking neural networks: Bringing the power of gradient-based optimization to spiking neural networks, IEEE Signal Processing Magazine 36 (6) (2019) 51–63.
- [27] P. J. Werbos, Backpropagation through time: what it does and how to do it, Proceedings of the IEEE 78 (10) (1990) 1550–1560.
- [28] B. Yin, F. Corradi, S. M. Bohté, Accurate and efficient time-domain classification with adaptive spiking recurrent neural networks, Nature Machine Intelligence 3 (10) (2021) 905–913.
- [29] W. Fang, Z. Yu, Y. Chen, T. Huang, T. Masquelier, Y. Tian, Deep residual learning in spiking neural networks, Advances in Neural Information Processing Systems 34 (2021) 21056–21069.
- [30] Y. Kim, J. Chough, P. Panda, Beyond classification: Directly training spiking neural networks for semantic segmentation, Neuromorphic Computing and Engineering 2 (4) (2022) 044015.
- [31] S. R. Kheradpisheh, T. Masquelier, Temporal backpropagation for spiking neural networks with one spike per neuron, International Journal of Neural Systems 30 (06) (2020) 2050027.

- [32] S. Zhou, X. Li, Y. Chen, S. T. Chandrasekaran, A. Sanyal, Temporal-coded deep spiking neural network with easy training and robust performance, in: Proceedings of the AAAI Conference on Artificial Intelligence, Vol. 35, 2021, pp. 11143–11151.
- [33] E. Ferrara, O. Varol, C. Davis, F. Menczer, A. Flammini, The rise of social bots, Communications of the ACM 59 (7) (2016) 96–104.
- [34] S. Cresci, R. Di Pietro, M. Petrocchi, A. Spognardi, M. Tesconi, The paradigm-shift of social spambots: Evidence, theories, and tools for the arms race, in: Proceedings of the 26th International Conference on World Wide Web Companion, 2017, pp. 963–972.
- [35] C. A. Davis, O. Varol, E. Ferrara, A. Flammini, F. Menczer, BotOrNot: A system to evaluate social bots, in: Proceedings of the 25th International Conference Companion on World Wide Web, 2016, pp. 273–274.
- [36] J. Rodríguez-Ruiz, J. I. Mata-Sánchez, R. Monroy, O. Loyola-Gonzalez, A. López-Cuevas, A one-class classification approach for bot detection on Twitter, Computers & Security 91 (2020) 101715.
- [37] A. Minnich, N. Chavoshi, D. Koutra, A. Mueen, BotWalk: Efficient adaptive exploration of Twitter bot networks, in: Proceedings of the 2017 IEEE/ACM International Conference on Advances in Social Networks Analysis and Mining 2017, 2017, pp. 467–474.
- [38] M. Balaanand, N. Karthikeyan, S. Karthik, R. Varatharajan, G. Manogaran, C. B. Sivaparthipan, An enhanced graph-based semi-supervised learning algorithm to detect fake users on Twitter, The Journal of Supercomputing 75 (2019) 6085–6105.
- [39] Q. Cao, M. Sirivianos, X. Yang, T. Pregueiro, Aiding the detection of fake accounts in large scale social online services, in: Presented as part of the 9th USENIX Symposium on Networked Systems Design and Implementation (NSDI 12), 2012, pp. 197–210.

- [40] N. Chavoshi, H. Hamooni, A. Mueen, Identifying correlated bots in Twitter, in: Social Informatics: 8th International Conference, SocInfo 2016, Bellevue, WA, USA, November 11-14, 2016, Proceedings, Part II 8, Springer, 2016, pp. 14-21.
- [41] S. Gupta, P. Kumaraguru, T. Chakraborty, MalReG: Detecting and analyzing malicious retweeter groups, in: Proceedings of the ACM India Joint International Conference on Data Science and Management of Data, 2019, pp. 61–69.
- [42] J. Pan, Y. Liu, X. Liu, H. Hu, Discriminating bot accounts based solely on temporal features of microblog behavior, Physica A: Statistical Mechanics and its Applications 450 (2016) 193–204.
- [43] H. S. Dutta, A. Chetan, B. Joshi, T. Chakraborty, Retweet us, we will retweet you: Spotting collusive retweeters involved in blackmarket services, in: 2018 IEEE/ACM International Conference on Advances in Social Networks Analysis and Mining (ASONAM), IEEE, 2018, pp. 242–249.
- [44] S. Thorpe, J. Gautrais, Rank order coding, Computational Neuroscience: Trends in Research, 1998 (1998) 113–118.
- [45] M. Pabian, D. Rzepka, M. Pawlak, Supervised training of siamese spiking neural networks with Earth Mover's Distance, in: ICASSP 2022-2022 IEEE International Conference on Acoustics, Speech and Signal Processing (ICASSP), IEEE, 2022, pp. 4233–4237.